

Supplement of Geosci. Model Dev. Discuss., 8, 1639–1686, 2015
<http://www.geosci-model-dev-discuss.net/8/1639/2015/>
doi:10.5194/gmdd-8-1639-2015-supplement
© Author(s) 2015. CC Attribution 3.0 License.



Supplement of

Application of WRF/Chem version 3.4.1 over North America under the AQMEII Phase 2: evaluation of 2010 application and responses of air quality and meteorology–chemistry interactions to changes in emissions and meteorology from 2006 to 2010

K. Yahya et al.

Correspondence to: Y. Zhang (yang_zhang@ncsu.de)

Supplementary Material

1. Model Configuration

Both simulations are performed at a horizontal resolution of 36- km with 148×112 horizontal grid cells over a North America domain that covers the continental U.S. (CONUS) and parts of Canada and Mexico. The anthropogenic emissions used are based on the 2008 National Emission Inventory (NEI) from the United States Environmental Protection Agency (U.S. EPA) (Pouliot et al., 2014). Meteorological ICONs and BCONs are from the National Center of Environmental Prediction's (NCEP) final reanalysis (FNL) data. The chemical ICONs and BCONs are from the Monitoring Atmospheric Composition and Climate (MACC) model (<http://www.gmes-atmosphere.eu/>). More detailed description of the model configuration can be found in Yahya et al. (2014).

2. Emission Trends

Figure S1 shows annual mean hourly average emission changes for SO_2 , NO_x , VOCs, NH_3 , EC, and POA from 2010 to 2006. Figure S2 shows seasonal mean hourly average emission changes for VOCs and NH_3 from 2010 to 2006. Over land, most emissions show a decrease from 2006 to 2010 except for small areas and several point sources. Unlike the changes in the emissions of SO_2 and NO_x , NH_3 and VOCs emissions exhibit strong seasonal variations in the emission trends, as shown in Figure S2. In JFD, NH_3 emissions decrease over southeastern and Midwest U.S., while NH_3 emissions increase significantly over northeastern U.S. and in parts of CA possibly due to increased downward radiation which contributes to NH_3 volatilization (EPA, 2004). For the other seasons, NH_3 emissions generally decrease over the whole of continental U.S. (CONUS) due to a decrease in animal population numbers (EPA, 2004). VOC emissions largely decrease in March, April, May (MAM) and January, February, and December (JFD), and increase in June, July, August (JJA) and September, October, and November (SON), especially in southeastern U.S.

3. ICONs/BCONs

The skin temperature and soil moisture initial conditions are important as they affect latent and sensible heat, which in turns affect the properties of the boundary layer. Figure S3 shows skin temperature and soil moisture fraction in winter (JFD) and summer (JJA) between 2010 and 2006 extracted from NCEP as boundary conditions for WRF and WRF/Chem simulations. The JFD skin temperatures show a significant decrease of up to -8°C over eastern and central U.S. and a moderate increase over western U.S. The JJA skin temperatures show a moderate overall increase over eastern and southern U.S. and a moderate decrease in western and northwestern U.S. The soil moistures show less variability from 2006 to 2010. General trends include an increase in soil moisture fraction over southeastern and central U.S. and a decrease over the northeastern and northwestern U.S. for JFD. For JJA, soil moisture fraction mainly decreases over eastern U.S. except for parts of Georgia, Alabama, and Mississippi. Large increases in soil moisture fraction are found over northern U.S. and parts of Canada and Mexico. Soil moisture and temperature are important variables in regulating the sensible and latent heat fluxes from the ground to the atmosphere, affecting wind speeds and planetary boundary layer height (PBLH). The accuracy of soil moisture initialization is important as latent heat fluxes are very sensitive to variations of soil moisture fraction. Latent heat fluxes tend to be overestimated when soil moisture fraction is high (Hong et al., 2009).

4. Model Evaluation

Figure S4 shows the spatial distribution of NMB plots for JFD and JJA 2006 and 2010 for T2 based on evaluation against CASTNET and SEARCH. T2 is generally more underpredicted by the model during the winter months compared to the summer months.

Figure S6 shows the spatial distributions of the average OC concentrations for the months during which the field data were collected during the periods specified in Figure 9 in 2006 and 2010. 2006 in general has higher OC concentrations compared to 2010. Southeastern U.S., also in general has higher OC concentrations compared to western U.S for both 2006 and 2010. The model severely underestimates OC concentrations over western U.S., with a maximum mean in downtown LA area of $1.5 - 1.8 \mu\text{g m}^{-3}$, when the observed OC concentrations for Pasadena and Bakersfield range from 1 to $8 \mu\text{g m}^{-3}$. Figure S5 also shows that the simulated OC concentrations do not change much daily with the variations in the observed OC concentrations, but remain low throughout the two months. Also, the observed OC concentrations at both sites in CA are much higher than those of SOA, indicating the dominance of POA for 2010 in western U.S. Although simulated SOA gives relatively better performance against observed SOA, OC is significantly underpredicted mainly because of significant underpredictions of POA (due to underestimate in POA emissions) that dominates OC concentrations. The underpredictions in SOA also contribute in part to the OC underpredictions. There would be additional uncertainties in using 1.4 as the factor for deriving OA concentrations from OC; however, and such uncertainties cannot explain the large discrepancies between the simulated and observed OC concentrations in 2010. In addition, stronger wind speeds from the model in JJA 2010 as shown in Figure S5 can help disperse OC over western U.S. toward further inland compared to the weaker winds over western U.S. in JJA 2006, reducing OC concentrations over western U.S in JJA 2010. Figure S6 also shows the spatial distribution of the concentrations of anthropogenic SOA (ASOA) and total SOA (TSOA) (=ASOA + BSOA) and the ratio of SOA/OA. The ratios for April to December 2006 range from 0 to 0.8 with higher ratios in southern U.S. from Nevada in the west to Virginia in the east, while the ratios for May to June 2010 range from 0 to 0.9 with higher ratios in eastern U.S. Table 1 also shows that the 2010 simulation has negative NMBs of -30% and -12% for OC at the IMPROVE

and STN sites, respectively. The statistics for CONUS are consistent with the underpredictions of OC at the above sites.

Table A1 shows the statistics for several meteorological, chemical and aerosol-cloud variables for the sensitivity simulations analyzed in Section 4.4 in the main paper. The 2006 baseline simulations are designated as Run 1, the 2010 baseline simulations are designated as Run 2, the sensitivity simulations using 2006 emissions but keeping all other inputs (e.g., meteorology and chemical ICONs/BCONs) and model set-up the same as Run 2 simulations are designated as Run 3, and the sensitivity simulations using 2006 chemical ICONs/BCONs keeping all other inputs and model set-up the same as Run 3 are designated as Run 4.

5. Changes in the concentrations of gas and PM species, the wind vector, and T2 from 2010 to 2006

As shown in Figure S7, SO₂ concentrations tend to decrease for all seasons at most locations (except for several locations in western U.S. in JJA, SON and JFD) over CONUS due to the decrease in SO₂ emissions. The slight increase in SO₂ concentrations over northwestern U.S. in JFD could be due to lower T2, reduced WS10 for dispersion, and decreased PBLH as shown in Figure S11. The slight increase in SO₂ concentrations over several locations in SON corresponds to the spatial pattern of reduced precipitation as shown in Figure S11. NO₂ concentrations in general decrease over most parts of CONUS except in parts of Canada in SON and JFD, and in largely populated areas in eastern U.S. in MAM. The large increases in NO₂ concentrations over Canada are a result of increases in NO₂ concentrations from the MACC BCONs, and not likely due to MACC ICONs. Jimenez et al. (2006) reported that a 48-hr spin-up time is sufficient to reduce the impact of ICONs to $\leq 10\%$ for O₃, but the impact of BCONs is more significant and persistent near domain boundaries, consistent with findings

from Samaali et al. (2009) and Schere et al. (2012). The 2010 – 2006 increase in NO_2 concentrations over urban areas in eastern U.S. in MAM could be due to a few reasons. Figure S1 shows a decrease in NO_x emissions; however, the decrease in NO_2 emissions over eastern U.S. is very small compared to the decrease in nitrogen oxide (NO) emissions (figure not shown), which had a maximum decrease of $\sim 15 \text{ mol km}^2 \text{ hr}^{-1}$ over eastern U.S. In addition to the decrease in NO emissions, it could also signify decreased photolytic conversion from NO_2 to NO due to a decrease in SWDOWN. Less NO_2 could also have been converted into nitrate radical (NO_3) due to decreased OH concentrations, as Table 1 also shows an overall decrease in NO_3 concentrations. The NO_2 hotspots also correlate to the decrease in O_3 concentrations in urban areas. This could indicate an increased titration of O_3 by NO. This is an important result for policy implications, as reducing NO_x emissions may reduce NO_2 concentrations overall for CONUS, but may not reduce NO_2 concentrations in several areas, especially in urban areas due to a combination of titration and complex interplay with local meteorology. NH_3 mixing ratios generally decrease in the U.S., except over the eastern U.S. in MAM and SON, where there are increases. NH_3 emissions decrease however, over eastern U.S. for all seasons. The increase in NH_3 concentrations in MAM and SON could be attributed to a number of reasons. Concentrations of NH_4^+ decrease for all seasons over eastern U.S. with the largest decreases in MAM and JJA. This could mean that less NH_3 is converted to NH_4^+ , especially for MAM and SON over eastern U.S. due to increases in T2 (as shown in Figure S11), which shifts the partitioning towards the gas-phase rather than the particulate phase. Second, as shown in Figures 11 and A4, SO_4^{2-} concentrations decrease the most over eastern U.S. in SON, which means that less NH_4^+ is needed to neutralize SO_4^{2-} . As shown in Figures S8 and S9, nitric acid (HNO_3) concentrations decrease over eastern U.S. in MAM and SON. The decrease in HNO_3 concentrations results in decreases in NO_3^- concentrations over eastern U.S., which means that less NH_4^+ is used up in neutralizing NO_3^- . Less NH_4^+ required for neutralization

would mean that more NH_3 remained in the gas phase. Third, as shown in Figure S12, wind speeds decrease over eastern and southeastern U.S. for MAM and SON, respectively, in 2010 compared to 2006, which could result in less dispersion of NH_3 concentrations over eastern U.S. In JJA and SON, high OM concentrations in Canada are attributed to the enhanced impacts of BCONs in JJA by increasingly convergent flow in this region. OM is made up of both POA and SOA. An increase in VOC emissions in eastern U.S. in MAM and SON leads to increases in OM concentrations. Decreases in VOC emissions in western U.S. for all seasons lead to decreases in OM concentrations. The OM concentrations in some areas do not follow a linear relationship with VOC emissions, however, such as southeastern U.S. in JJA, where VOC emissions increase from 2006 to 2010 but OM concentrations decrease. A decrease in POA concentrations must dominate the overall decrease in OM concentrations, even under increased temperatures and biogenic VOC emissions in this area. $\text{PM}_{2.5}$ concentrations decrease for all seasons and most regions of the CONUS, which is attributed mainly to decreases in precursor gases, especially the inorganic precursors SO_2 and NO_x in eastern U.S. Increased $\text{PM}_{2.5}$ concentrations in JFD and MAM in the Midwest are due to surface temperature decreases, dominating in this region (Stoeckenius et al., 2014). This in turn leads to increased particle nitrate concentrations (Campbell et al., 2014).

6. Differences between predictions of meteorological variables by WRF/Chem and WRF

Figures A10 and A11 show absolute differences between predictions of meteorological variables by WRF and WRF/Chem (2010 – 2006), respectively. The spatial patterns between the differences in meteorological variables T2, WS10, PBLH and Precip from 2006 and 2010 are similar for WRF and WRF/Chem, though differences in magnitudes of the variables can be seen. These

differences are quantified in Figure S13, which shows absolute differences between predictions of meteorological variables by WRF/Chem and WRF (WRF/Chem – WRF) simulations for 2010. Figure S12 compares wind vectors superposed with T2 in 2006 and 2010 from WRF/Chem and shows the largest differences in wind vectors are in JJA. JJA 2006 has strong northwesterly winds over the coast in the northwestern portion of the domain while for JJA 2010 over the same area the winds are weak and westerly. Over the coast in the eastern portion of the domain, winds are southerly for JJA 2006 but westerly for JJA 2010. For SON, off the eastern coast, the westerly winds are stronger for 2010 compared to 2006. Other than these obvious differences, the seasonally averaged wind patterns are similar for 2006 and 2010.

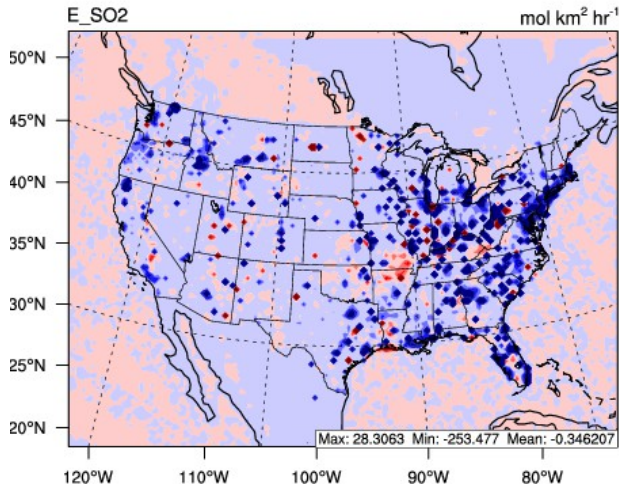
Additional references

Hong, S., Lakshmi, V., Small, E.E., Chen, F., Tewari, M., Manning, K.W., 2009. Effects of vegetation and soil moisture on the simulated land surface processes from the coupled WRF/Noah model. *J. Geophys. Res.*, 114, D18118, doi:10.1029/2008JD011249.

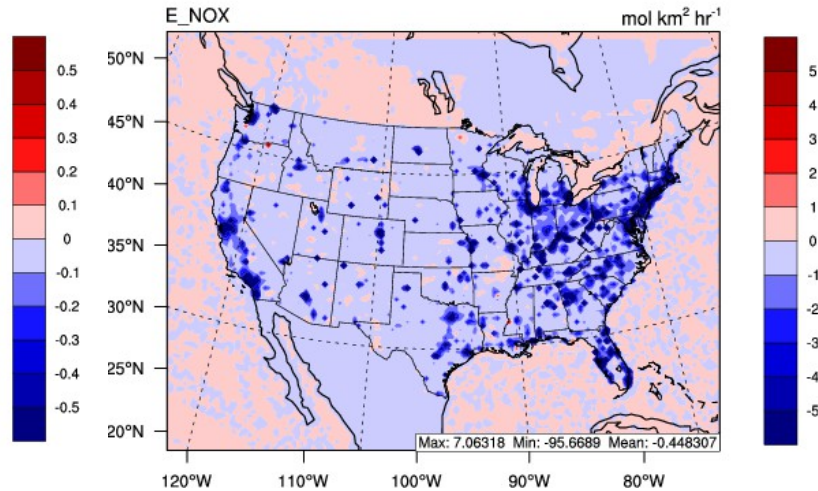
Table S1. Summary of statistics for several meteorological, chemical and cloud-aerosol variables for the sensitivity simulations.

	RUN 1			RUN 2			RUN 3			RUN 4		
	NMB (%)	NME (%)	Corr									
CASTNET T2 (Jan)	-75.3	143.0	0.90	57.3	-375.8	0.59	50.4	-195.9	0.91	49.8	-195.6	0.91
CASTNET SWDOWN (Jan)	15.6	38.5	0.92	49.2	83.3	0.75	14.6	70.1	0.77	14.9	70.3	0.77
MODIS CF (Jan)	-5.4	12.8	0.85	-3.2	11.4	0.87	-3.4	10.6	0.87	-3.4	10.6	0.87
MODIS COT (Jan)	-65.5	65.6	0.58	-64.5	64.9	0.35	-63.7	64.2	0.35	-63.6	64.1	0.35
MODIS AOD (Jan)	-45.8	58.9	-0.05	-47.9	57.8	-0.05	-37.5	56.9	-0.08	-30.6	53.7	-0.10
Max 8-hr O₃ (Jan)	-21.5	26.0	0.74	-29.2	32.0	0.54	-37.8	38.8	0.66	-19.6	25.8	0.62
PM_{2.5} (Jan)	-30.5	55.5	0.29	-17.2	68.7	-0.11	-19.0	49.0	0.38	-18.2	49.2	0.38
CASTNET T2 (Jul)	-5.0	12.7	0.85	-2.9	13.3	0.80	-2.8	12.3	0.83	-2.8	12.2	0.83
CASTNET SWDOWN (Jul)	9.1	30.8	0.90	6.3	37.7	0.86	5.7	49.3	0.82	7.0	49.7	0.82
MODIS CF (Jul)	-0.4	20.8	0.72	-3.8	18.0	0.83	-3.7	18.0	0.83	-3.2	17.9	0.83
MODIS COT (Jul)	-61.3	64.3	0.36	-65.6	66.8	0.19	-68.2	71.0	0.12	-67.7	70.5	0.14
MODIS AOD (Jul)	-47.0	48.0	0.65	-16.1	43.4	0.25	-4.9	49.4	0.23	-20.0	52.1	0.21
Max 8-hr O₃ (Jul)	5.2	23.1	0.40	-10.8	23.1	0.41	-5.4	19.7	0.54	23.3	32.9	0.46
PM_{2.5} (Jul)	-15.0	43.5	0.43	-18.8	46.7	0.38	2.8	40.5	0.61	6.7	42.3	0.61

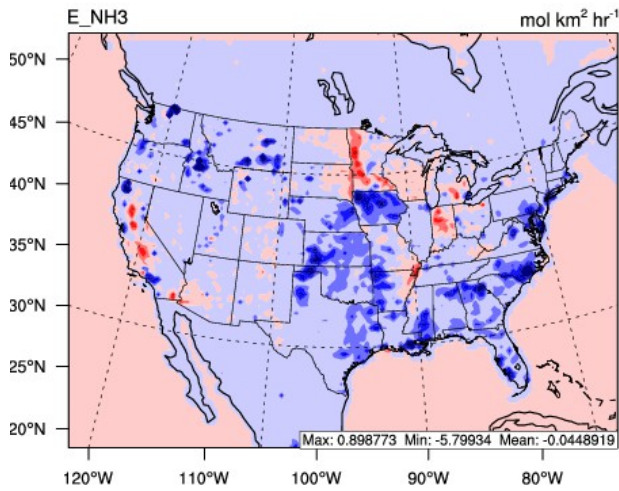
Annual 2010 - Annual 2006



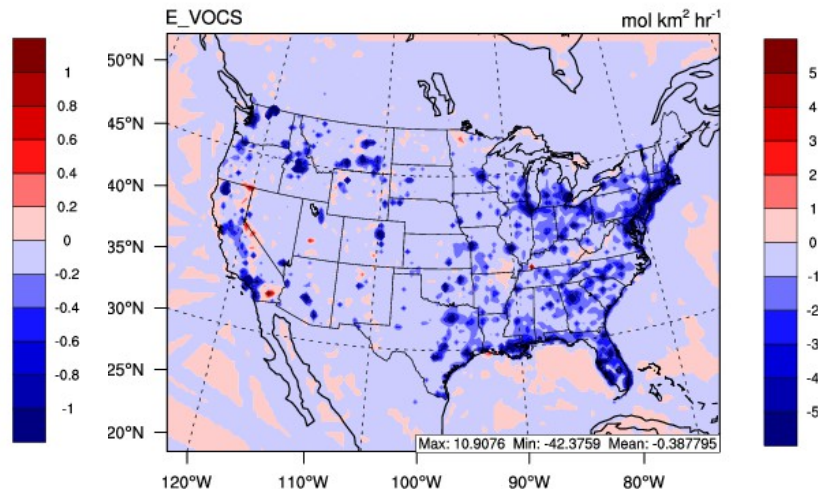
Annual 2010 - Annual 2006



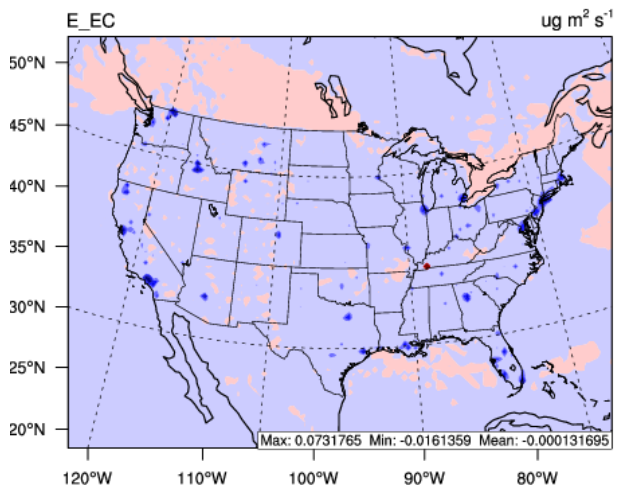
Annual 2010 - Annual 2006



Annual 2010 - Annual 2006



Annual 2010 - Annual 2006



Annual 2010 - Annual 2006

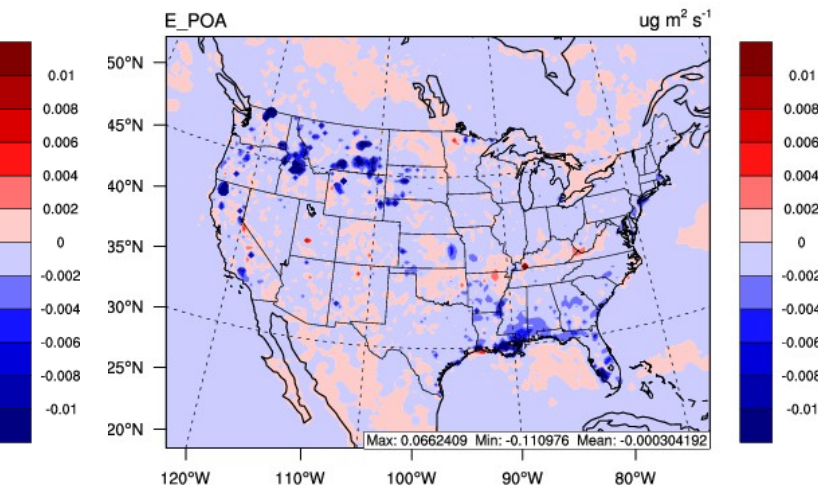


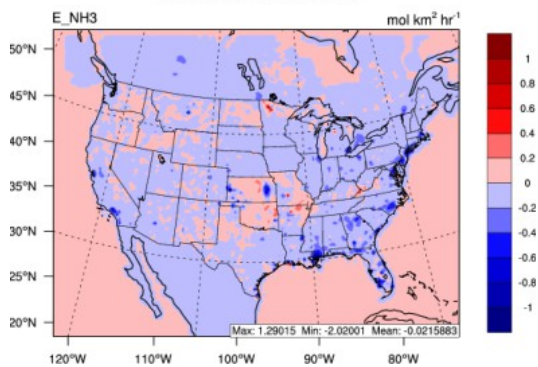
Figure S1. Annual mean changes in the hourly average emission for SO₂, NO_x, VOCs, NH₃, EC, and POA from 2010 to 2006 (2010 – 2006).

NH₃

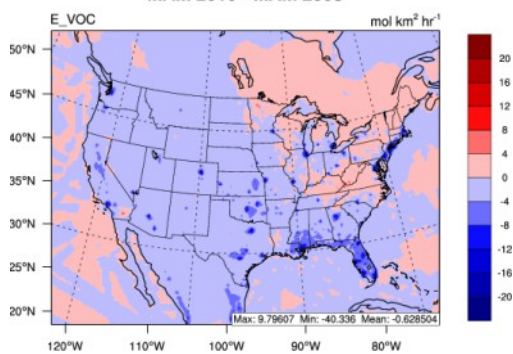
VOCs

MAM

MAM 2010 - MAM 2006

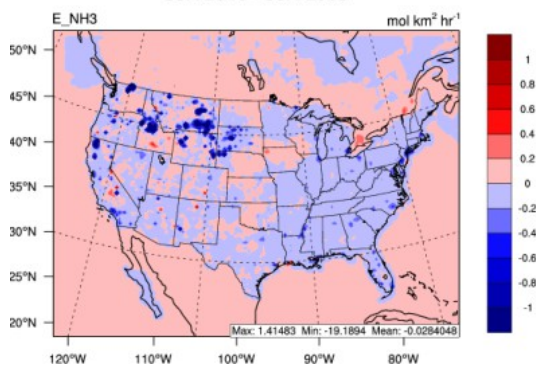


MAM 2010 - MAM 2006

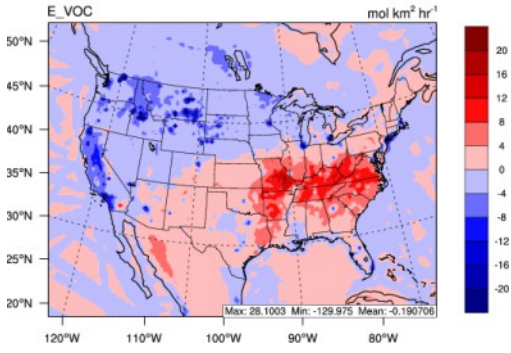


JJA

JJA 2010 - JJA 2006

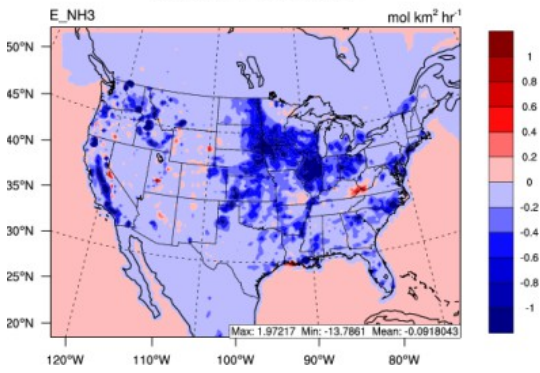


JJA 2010 - JJA 2006

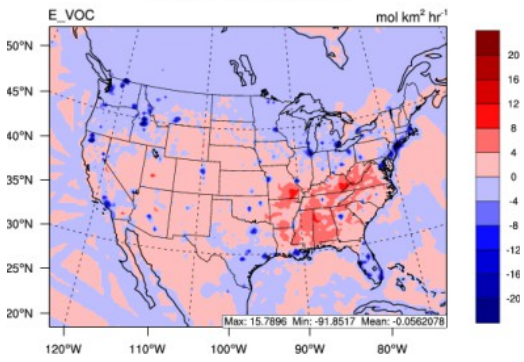


SON

SON 2010 - SON 2006



SON 2010 - SON 2006



JFD

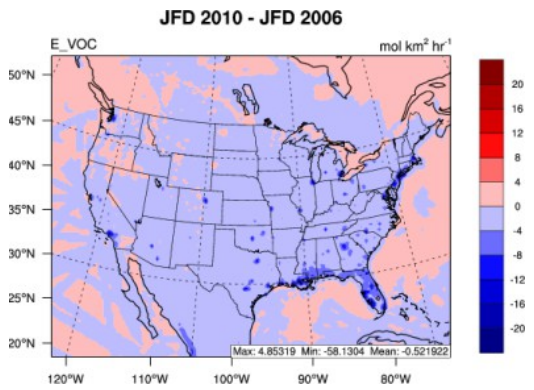
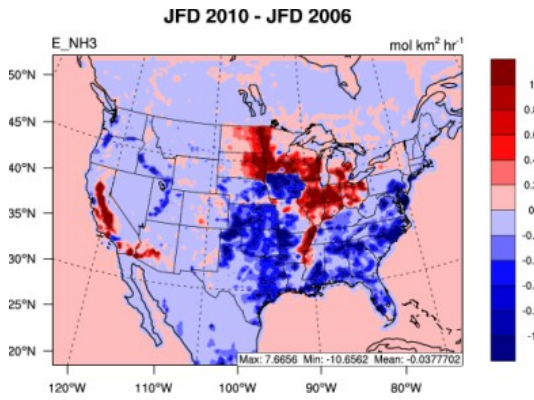
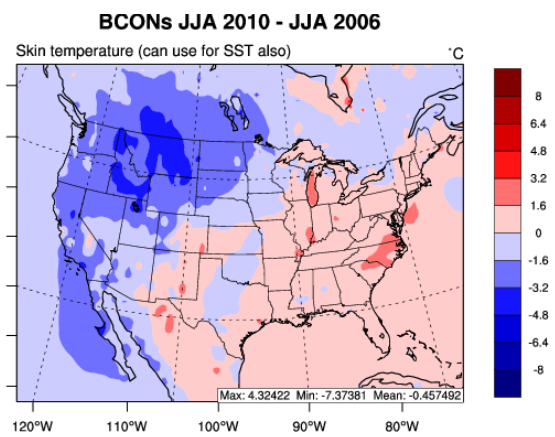
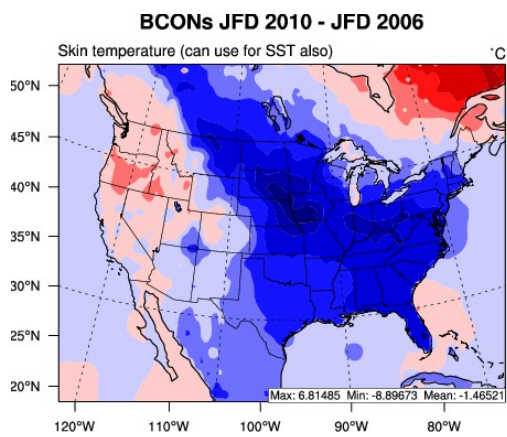


Figure S2. Hourly average emission changes for NH₃ and VOCs from 2010 to 2006 (2010 – 2006).



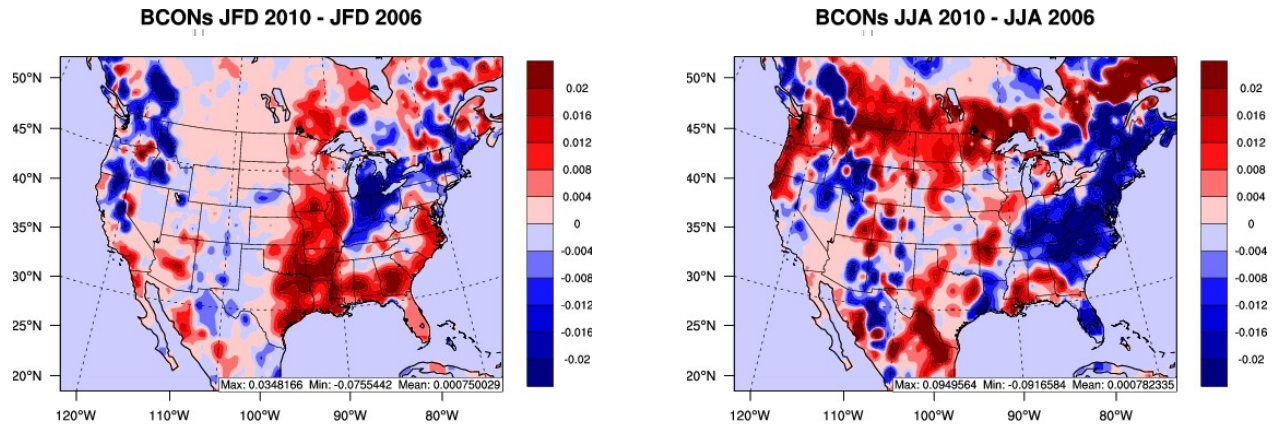
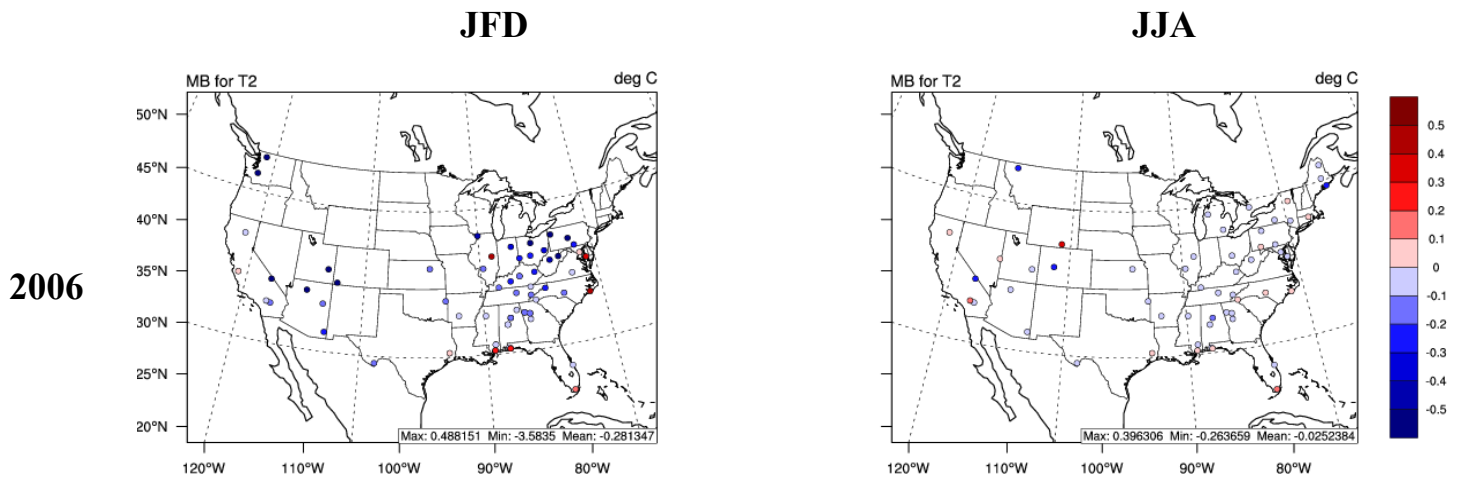


Figure S3. Differences in skin temperature and soil moisture fraction in winter (JFD) and summer (JJA) between 2010 and 2006 extracted from NCEP as boundary conditions for WRF and WRF/Chem simulations.



2010

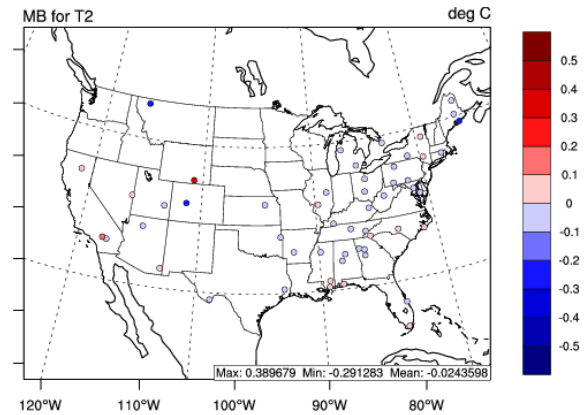
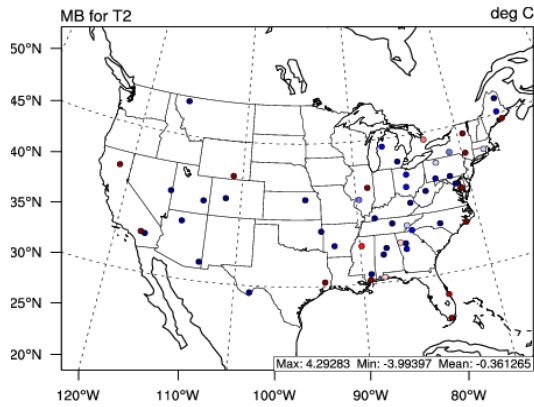
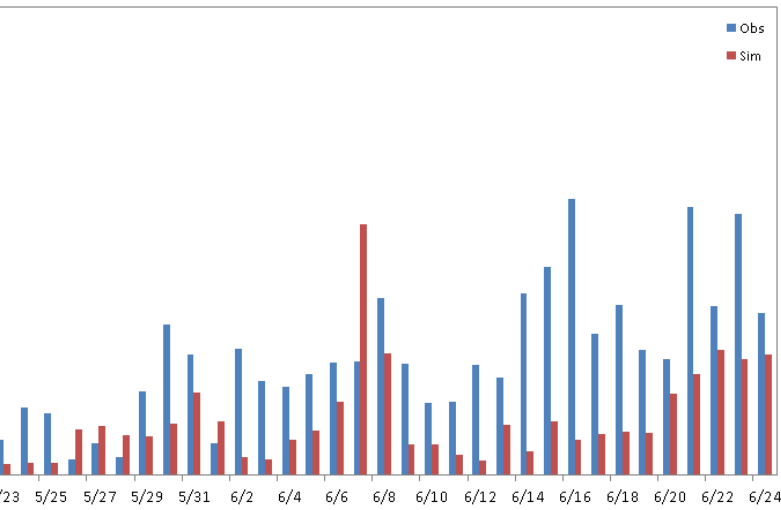
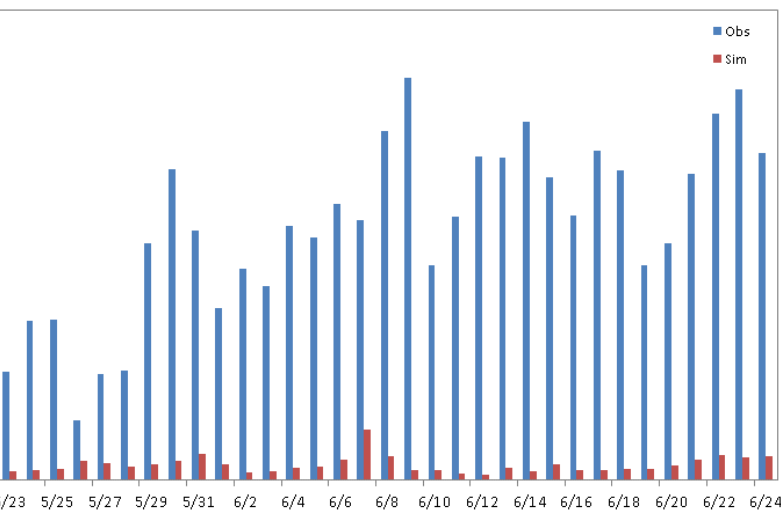
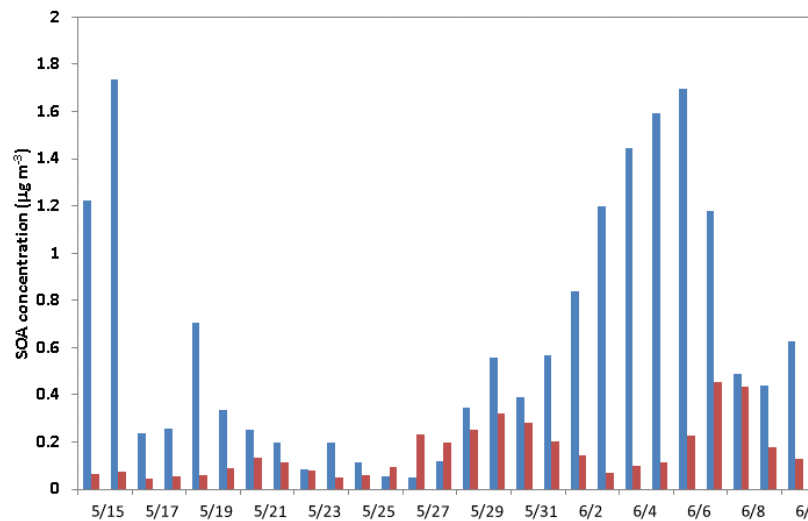


Figure S4. Spatial Distribution of MB plots for JFD and JJA 2006 and 2010 for T2 based on evaluation against CASTNET and SEARCH.

May – June 2010, Bakersfield, CA



May – June 2010, Pasadena, CA



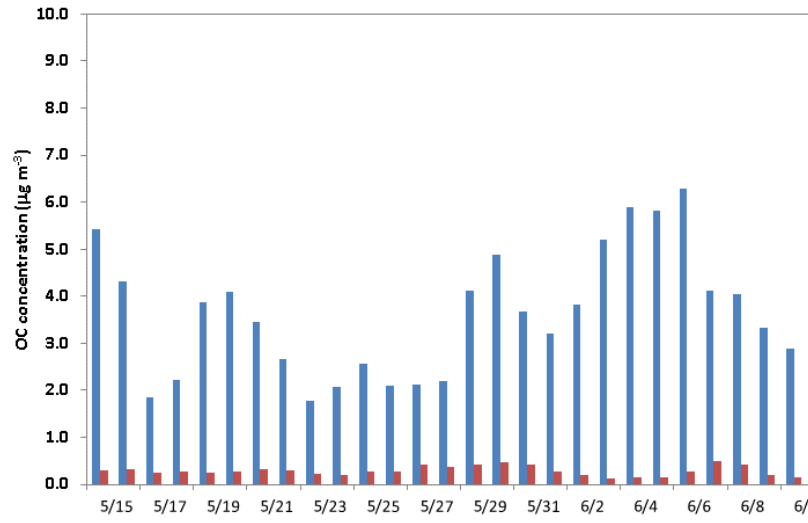


Figure S5. Column Plots of SOA and OC concentrations at Bakersfield, CA and Pasadena, CA from May – June 2010.

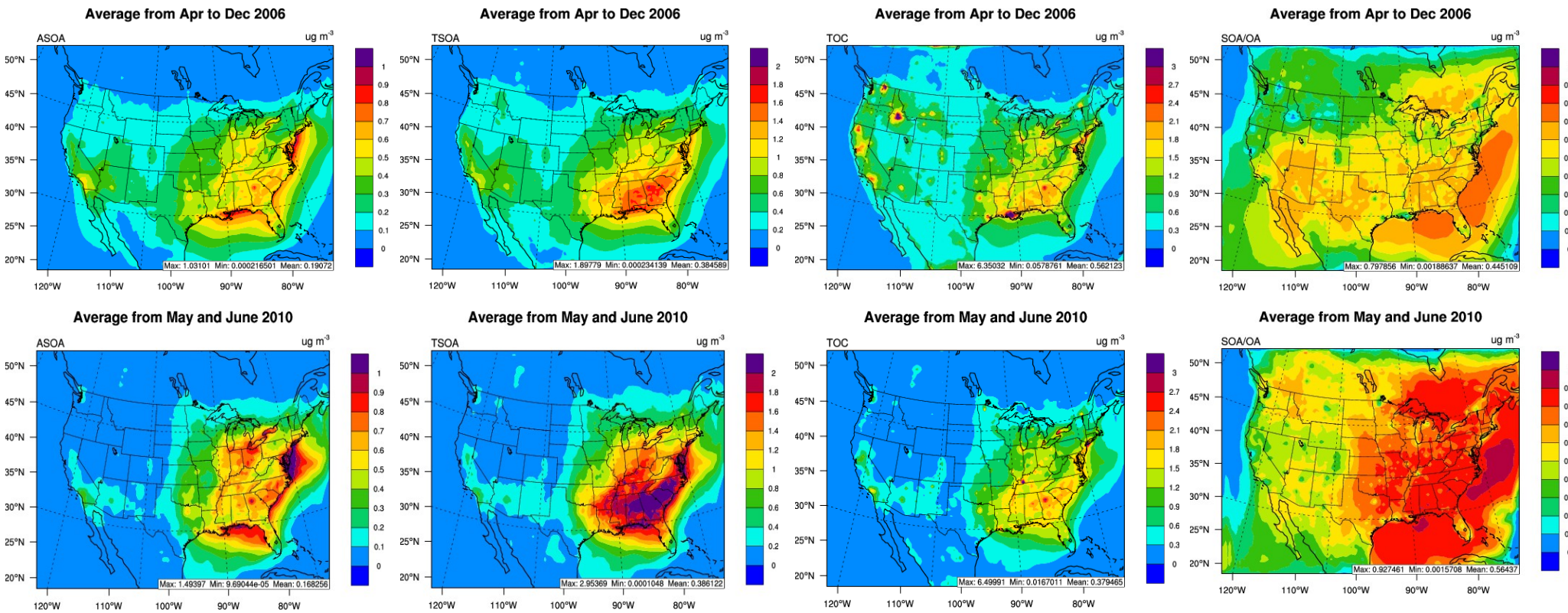


Figure S6. Spatial Distribution plots of average anthropogenic SOA (ASOA), total SOA (TSOA), total OC (TOC) and ratio of SOA/TSOA across months in 2006 and 2010 based on Figure 7.

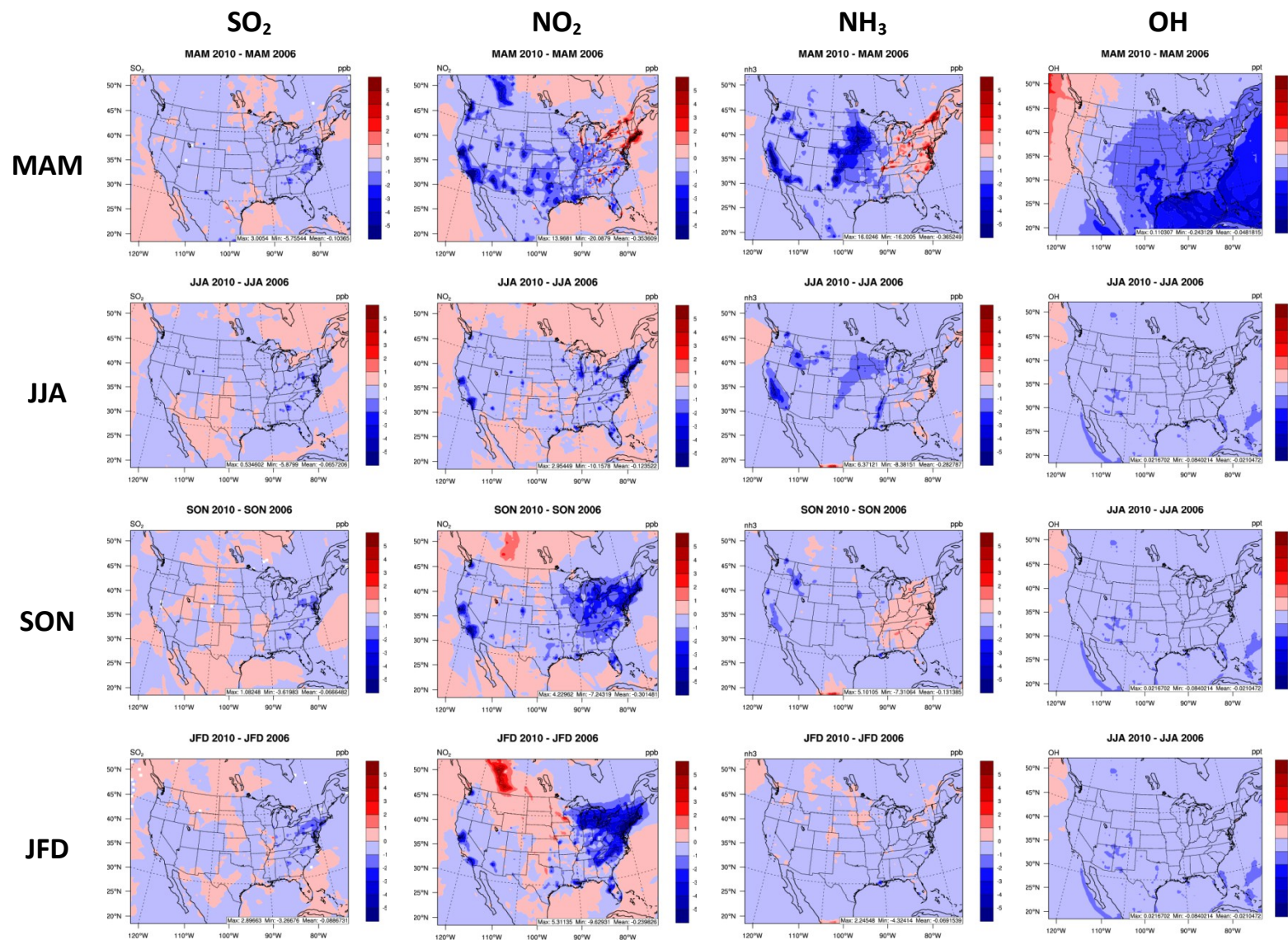


Figure S7. Changes in hourly average surface concentrations of selected gaseous species from 2010 to 2006 (2010 – 2006).

NH₄⁺

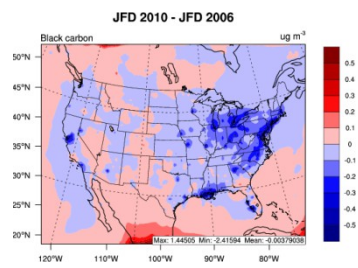
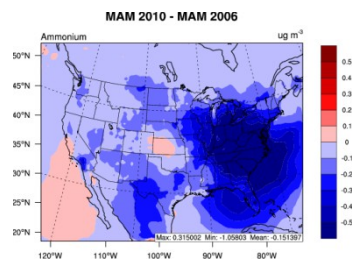
EC

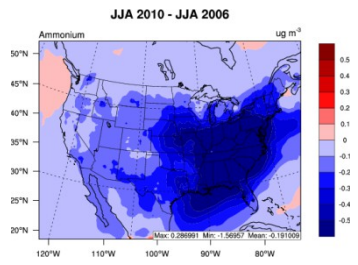
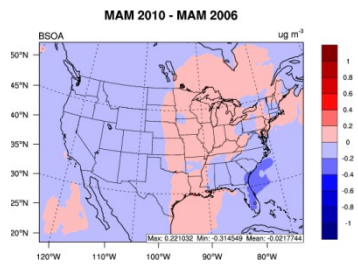
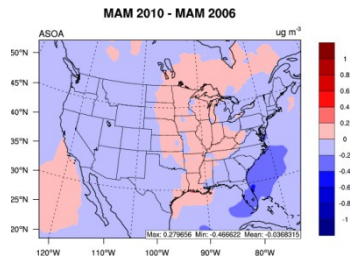
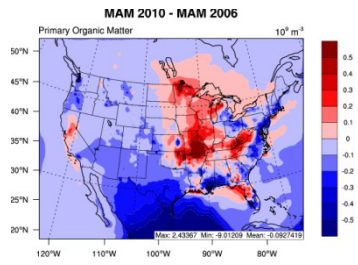
POA

ASOA

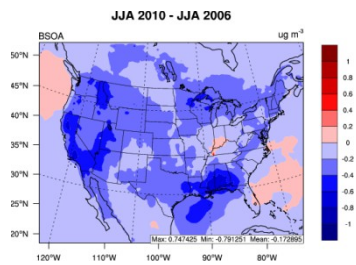
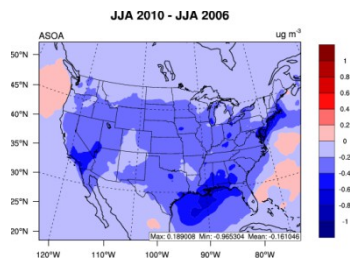
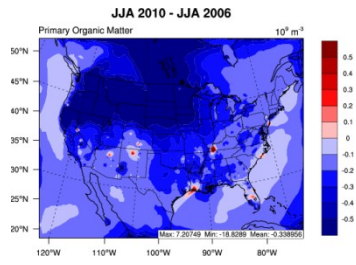
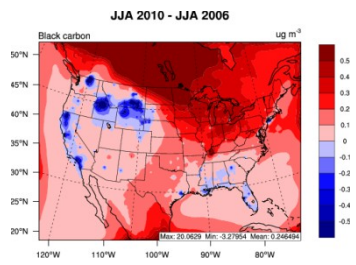
BSOA

MAM

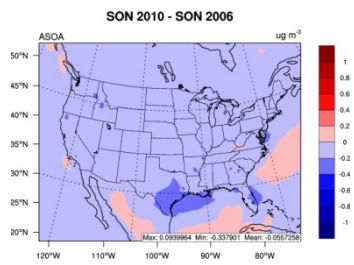
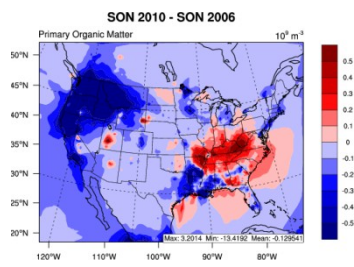
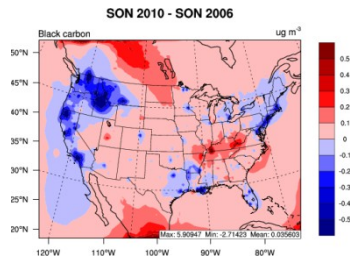
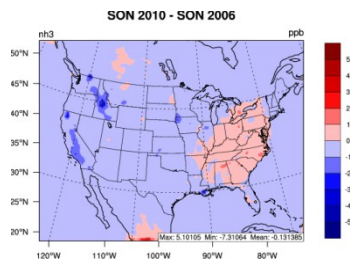


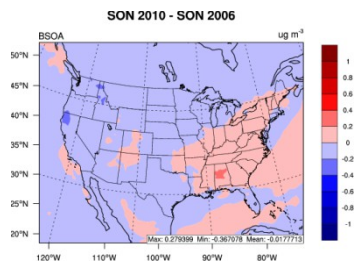


JJA

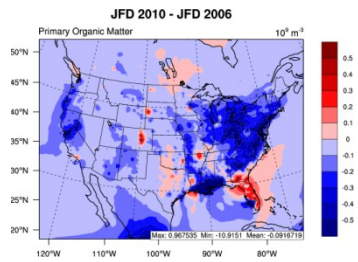
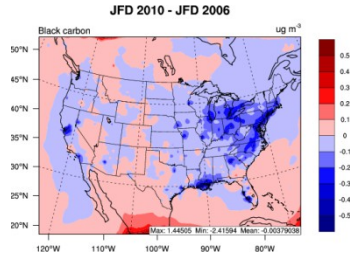
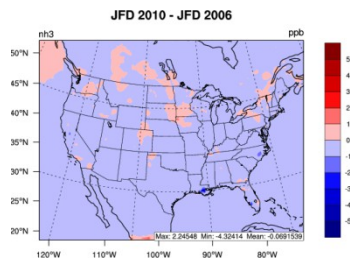


SON





JFD



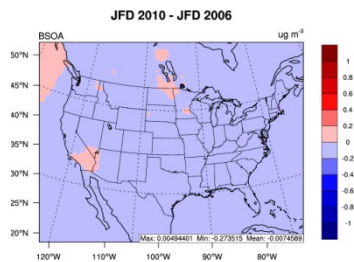
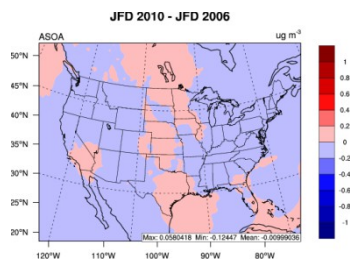
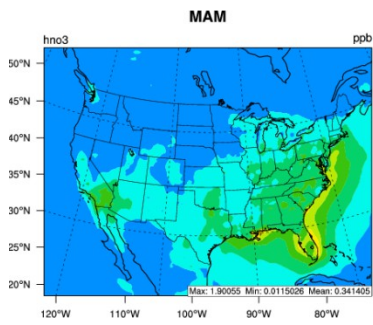
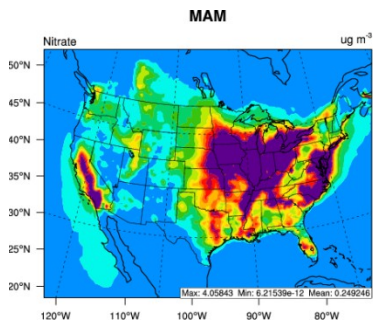
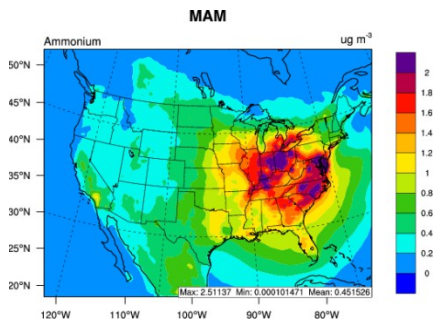


Figure S8. Changes in the hourly average surface concentration of selected PM species from 2010 to 2006 (2010 – 2006).

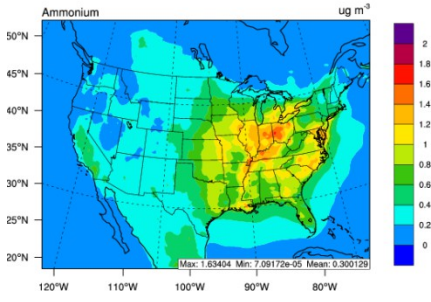


MAM2006

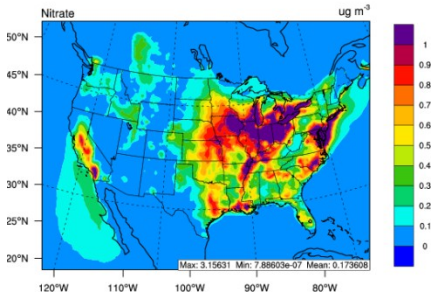


MAM2010

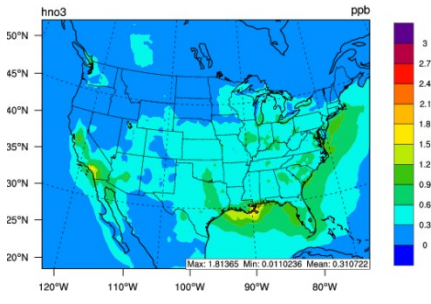
MAM 2010



MAM 2010

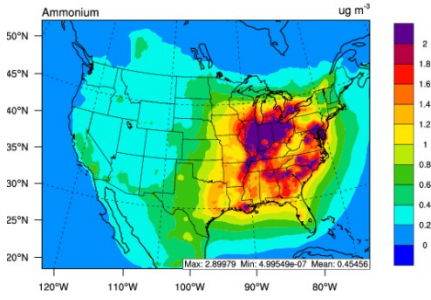


MAM 2010

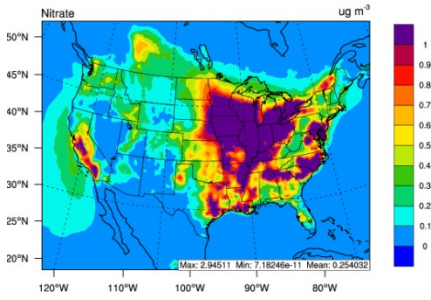


SON 2006

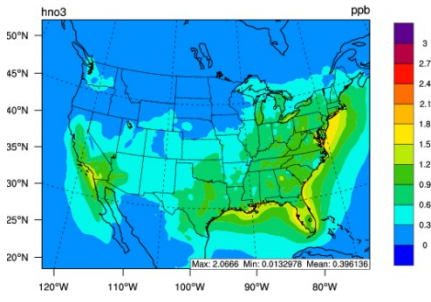
SON



SON

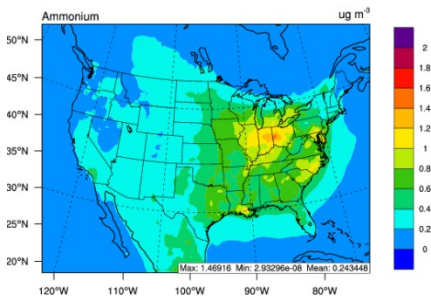


SON



SON 2010

SON 2010



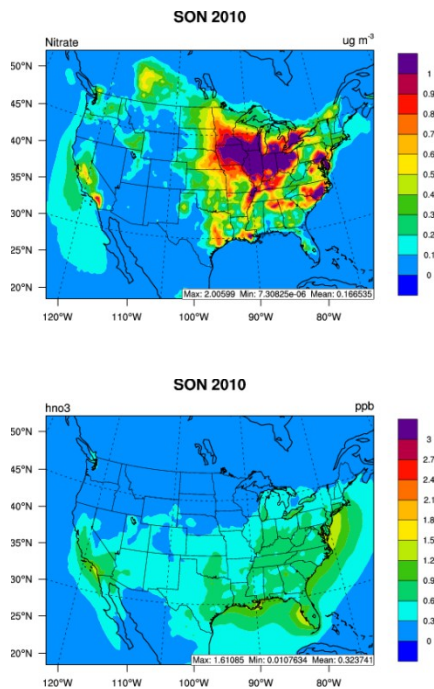


Figure S9. Ammonium, nitrate and nitric acid concentrations for MAM (top 2 rows) and SON 2006 and 2010 (bottom 2 rows).

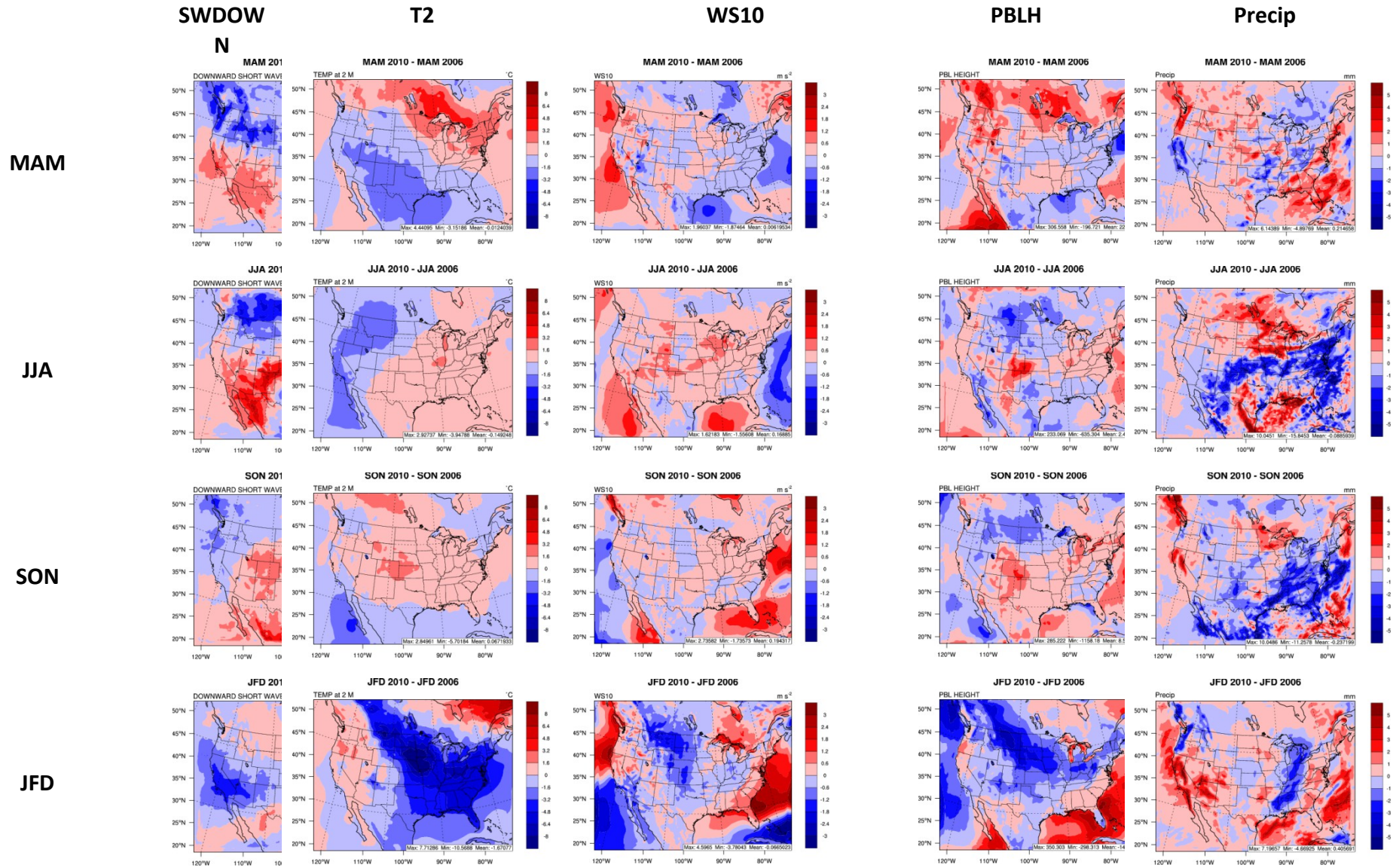


Figure S10. Hourly average changes for meteorological variables from WRF only simulations for 2010 to 2006 (2010 - 2006).

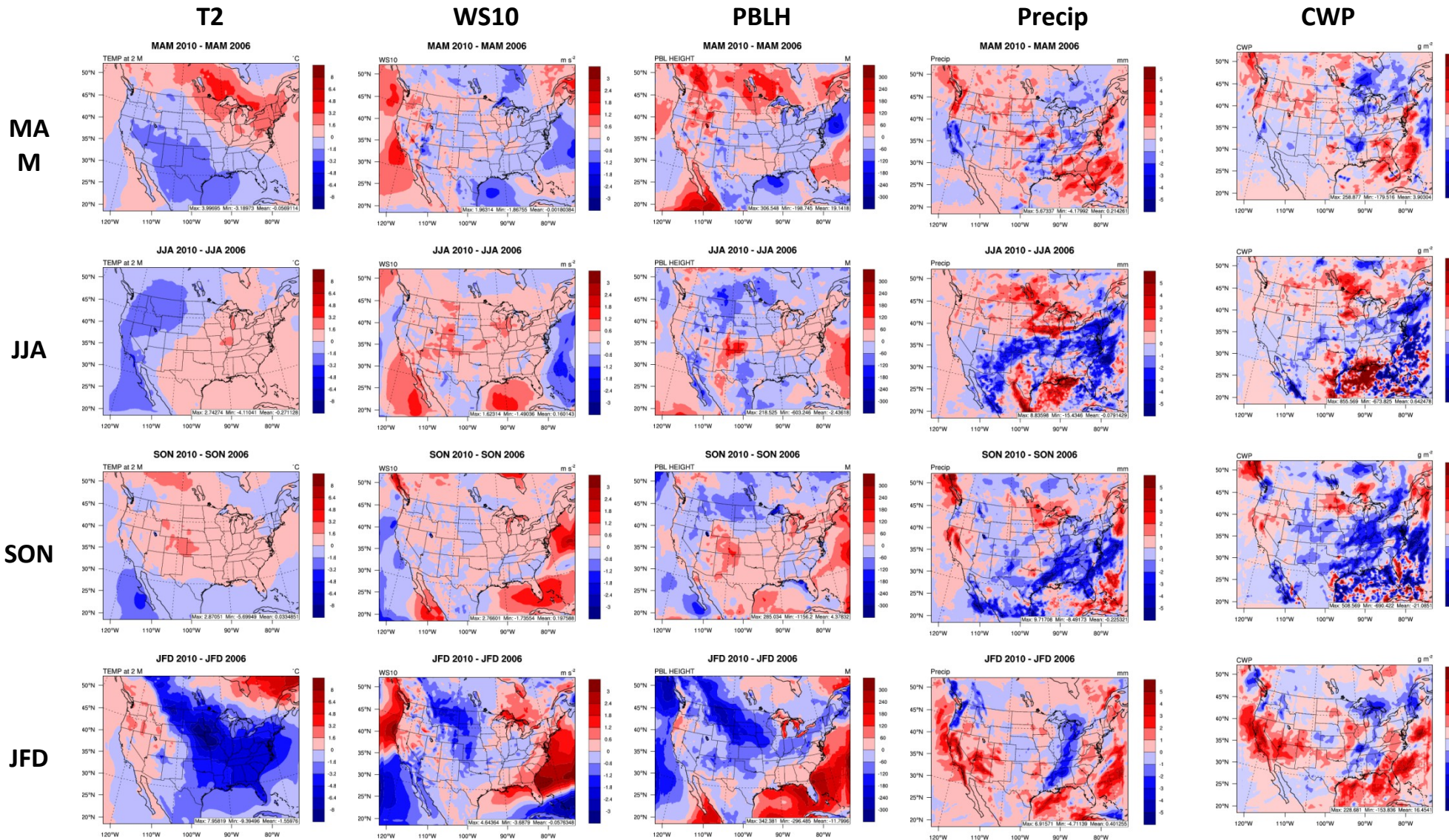
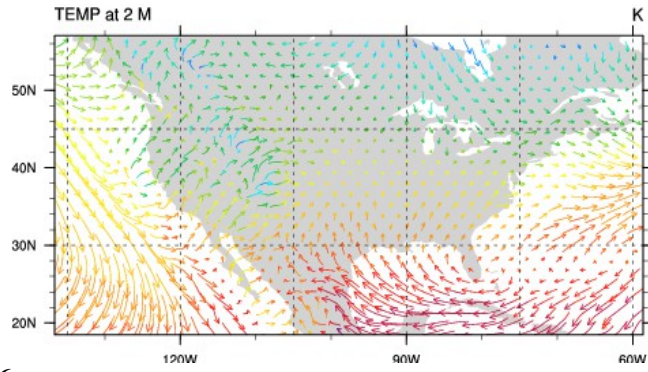
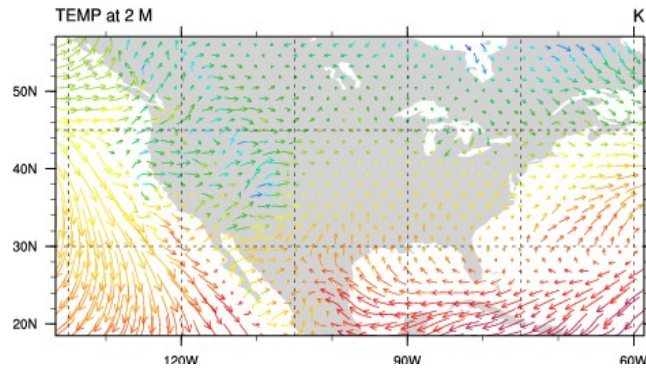


Figure S11. Changes in the hourly average surface predictions of meteorological variables from WRF/Chem simulations from 2010 to 2006 (2010 – 2006).

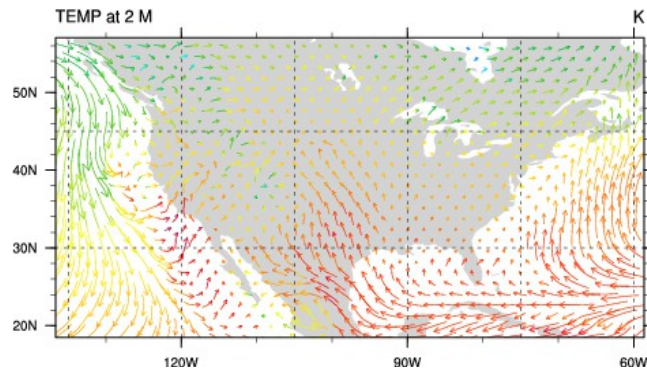


MAM 2006

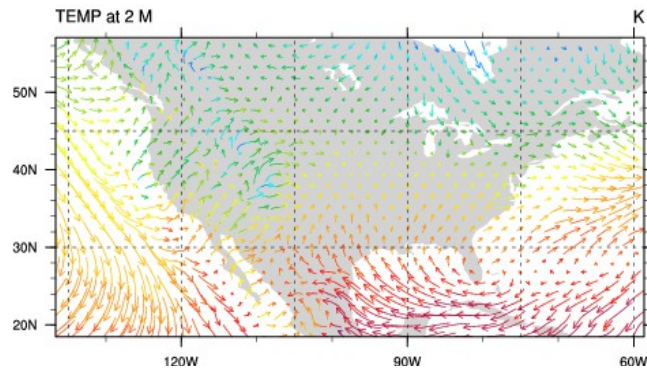
MAM 2010



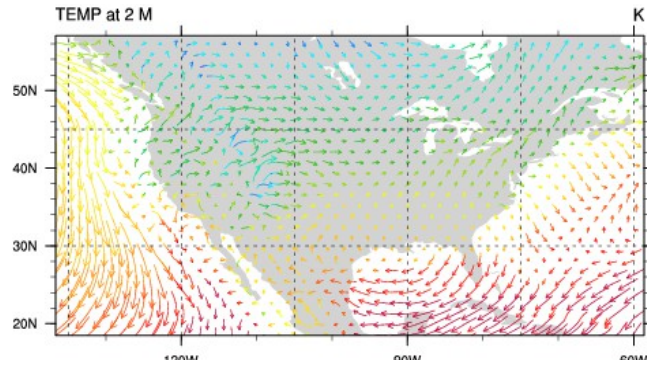
JJA 2006



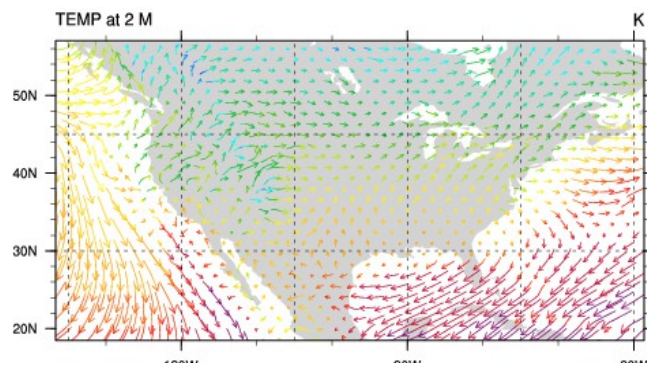
JJA 2010



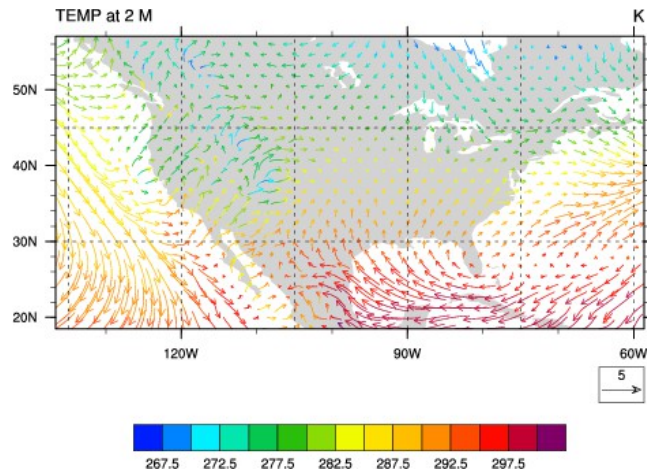
SON 2006



SON 2010



JFD 2006



JFD 2010

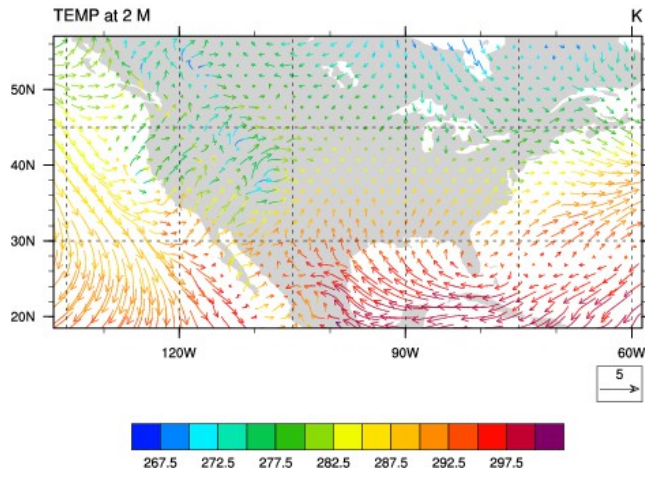


Figure S12. Wind vectors at 10-m and T2 by for all seasons for 2006 and 2010.

SWDOWN

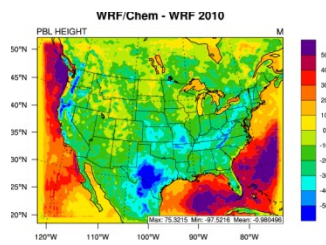
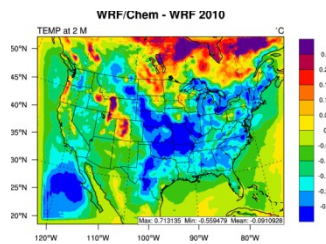
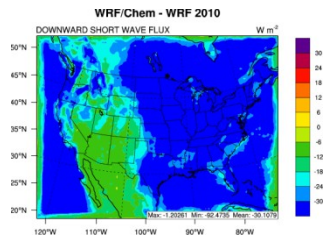
T2

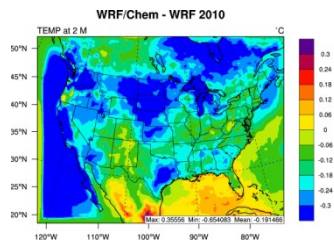
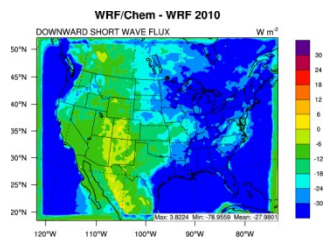
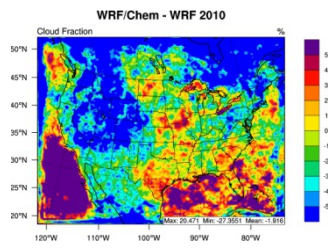
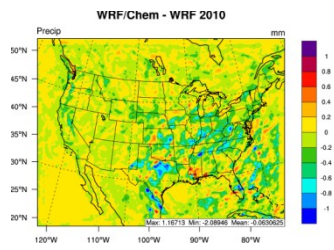
PBLH

Precip

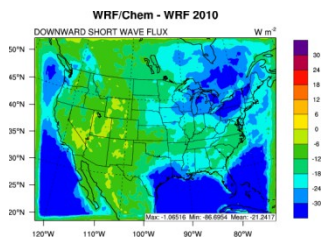
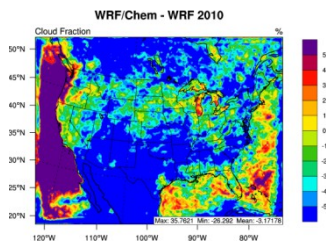
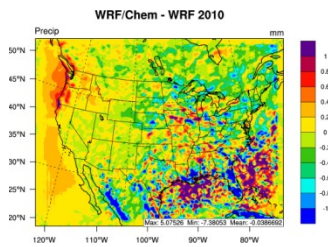
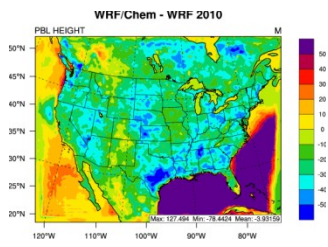
CF

MAM

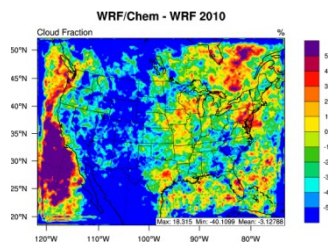
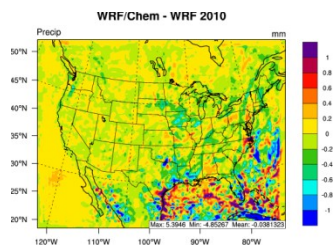
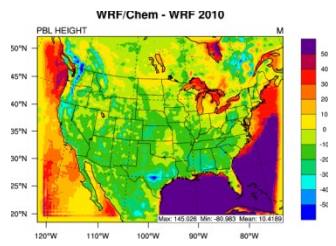
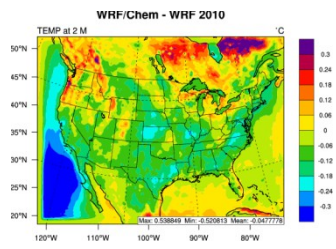




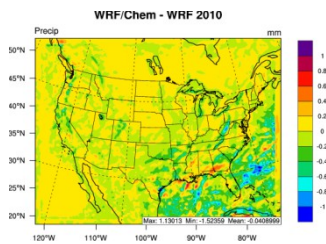
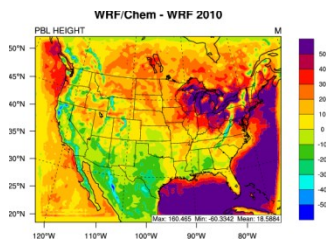
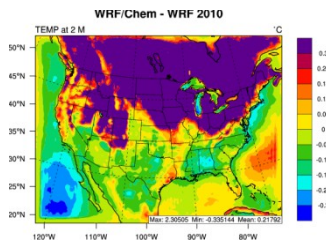
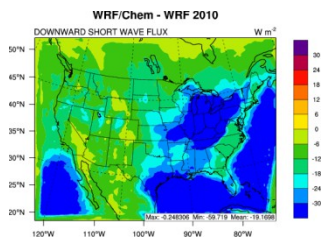
JJA



SON



JFD



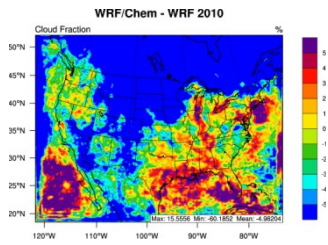


Figure S13. Absolute Differences between predictions of meteorological variables by WRF/Chem and WRF (WRF/Chem – WRF) simulations for 2010.